Diversity-Oriented Synthesis of Graft Copolymer Silicones Enables Exceptionally Broad Thermomechanical Property Windows through Pendant-Mediation

Keith Husted
Massachusetts Institute of Technology
Abraham Herzog-Arbeitman
Massachusetts Institute of Technology
Denise Kleinschmidt
Massachusetts Institute of Technology
Wenxu Zhang
Massachusetts Institute of Technology
Alyssa Fielitz
DOW
An Le
Yale University
Mingjiang Zhong
Yale University https://orcid.org/0000-0001-7533-4708
Jeremiah Johnson (jaj2109@mit.edu)
Massachusetts Institute of Technology https://orcid.org/0000-0001-9157-6491

Article

Keywords:

Posted Date: January 19th, 2022

DOI: https://doi.org/10.21203/rs.3.rs-1115203/v1

Abstract

Graft copolymers offer a versatile platform for the design of self-assembling materials; however, simple strategies for precisely and independently controlling the thermomechanical and morphological properties of graft copolymers over wide property windows remain elusive. Here, using a library of 92 systematically varied polynorbornene-graft-polydimethylsiloxane (PDMS) copolymers, we discover a versatile backbone-pendant sequence control strategy that overcomes this challenge. We find that small structural variations of aliphatic pendant groups, e.g., cyclohexyl versus n-hexyl, of small molecule comonomers have dramatic impacts on the order-to-disorder transitions, glass transitions, mechanical properties, and self-assembled morphologies of statistical and block silicone-based graft copolymers, providing an exceptionally broad palette of designable materials properties, e.g., elastic moduli that vary over 9 orders-of-magnitude. For example, statistical graft copolymers with very high PDMS volume fractions yielded unbridged body-centered cubic (BCC) morphologies that behaved as ultra-soft, shear-thinning, plastic crystals. By contrast, lamellae-forming statistical graft copolymers provided robust, stiff, yet reprocessable silicone thermoplastics (TPs) with transition temperatures spanning over 160 °C and elastic moduli as high as 150 MPa, which is much greater than commercial silicone thermosets. Altogether, this study reveals a new pendant-mediated assembly strategy that simplifies graft copolymer synthesis and enables access to a diverse family of silicone materials, setting the stage for the broader development of self-assembling materials with tailored performance specifications.

Main

Graft copolymers, which feature polymeric side chains attached to a polymer backbone, offer greater structural complexity than traditional linear (co)polymers, with parameters such as backbone length, sidechain sequence,[1–5] sidechain length,[6] grafting density,[7,8] and block lengths[9] defining their unique bulk properties[10–14] and self-assembled morphologies[15–21] and enabling their application as optical materials,[22,23] elastomers,[24–28] drug delivery systems,[29,30] biomimetics,[27,31–34] and more.[35–38] Nevertheless, despite enormous recent interest in their synthesis and properties, most studies of graft copolymers to date have involved either homopolymers or copolymers derived from two different polymer side chains arranged in either block or statistical sequences; the potential for combining graft polymer segments with small-molecule comonomers, leveraging only the latter to tune material properties, has been much less explored. Sheiko and coworkers reported A-B-A triblock copolymers with linear polymer A blocks and a graft copolymer B block; these structures formed very soft thermoplastic elastomers through microphase separation of their A blocks into spherical morphologies bridged by the B segment.[33] Bates and coworkers reported statistical graft copolymers featuring polydimethylsiloxane (PDMS) and smaller, oligoethylene oxide (OEO) side chains; intramolecular phase separation of the PDMS and OEO segments yielded very soft, shear thinning materials with unbridged spherical morphologies.[39] In a different vein, Grubbs and coworkers explored the impact of small molecule monomers as “diluents” in the formation of diblock bottlebrush copolymers, revealing how tapered and gradient sidechains can impact diblock bottlebrush assembly. While inspiring, these disparate studies do not explore the impact

of comonomer composition on the thermomechanical properties and morphologies of the materials investigated, relying primarily on tuning dimensions of the grafted chains to modulate material characteristics. Moreover, these studies do not provide access to a wide range of thermomechanical properties.

Here, we introduce a simple diversity-oriented synthetic platform for rapidly exploring and discovering graft copolymer-based silicone materials with diverse, bespoke properties. Silicones are an important category of commercial polymers that find numerous applications as lubricants, elastomers, sealants, components of household appliances, dielectrics and more, and are produced on the ~2 M ton scale annually. Despite their broad utility, however, silicones suffer from low moduli and difficult-to-tune thermal transitions, unless they are densely crosslinked or filled, two strategies which can be prohibitive in terms of material (re)processing, flexibility, and optical properties (e.g., transparency). These drawbacks motivated our interest in designing a modular, efficient synthetic approach to broadly tune silicone properties using a simple copolymerization strategy. Through ring-opening metathesis polymerization (ROMP) of an *exo*-norbornene-terminated PDMS macromonomer combined with one of three comonomers featuring aliphatic sidechains (*n*-hexyl, cyclohexyl, or *n*-hexadecyl), a library of 92 graft copolymers was prepared (**Fig. 1a**). Bulk samples from this library displayed a remarkable range of properties. For example, statistical copolymers with very high PDMS weight fractions (up to $f_{PDMS-MM}$ = 0.98) behaved as shear-thinning, soft (E' ~ 100 kPa) plastic crystals with body-centered cubic (BCC) spherical morphologies. By contrast, statistical copolymers with lower PDMS volume fractions (e.g., $f_{PDMS-MM}$ = 0.53) formed reprocessable TPs with lamellar morphologies, broad processing windows (over 160°C), and room temperature elastic moduli (E') ranging from 10 to 150 MPa, which are greater than leading unfilled commercial crosslinked silicone elastomers (e.g., Sylgard 184 with E' of 1.7 MPa).[40] Moreover, these graft copolymer silicones can be easily reprocessed to provide new materials with equivalent mechanical performance, offering a recyclable alternative to crosslinked silicone thermosets. Remarkably, the pendant groups of the small molecule comonomers are shown to play dominant roles in defining the thermomechanical and morphological properties of these materials, which has generally been overlooked in related studies. Meanwhile, as expected, domain spacing relationships are dictated by grafting density and backbone sequence, providing easily variable and independent parameters for controlling material structure and properties. Finally, we find that statistical copolymers, which are generated in a single polymerization step, provided materials with improved thermomechanical properties compared to block copolymers of the same $f_{PDMS-MM}$, which facilitates the scalability of these materials as demonstrated through decagram-scale syntheses.

Diversity-Oriented Synthesis of a Library of Graft Copolymer Silicones

PDMS-based macromonomer **Nb-PDMS** and small-molecule comonomers with aliphatic pendants **cHex**, **nHex**, and **nHexDec** were each prepared in a single step from the appropriate *exo*-norbornene electrophile and commercially available hydroxyl-terminated PDMS (5 kDa), hexylamine, cyclohexylamine, or hexadecylamine, respectively (**Fig. 1a**). Leveraging the robust nature of Ru-initiated ROMP,[41] a library of

92 unique (co)polymer compositions was prepared from these 4 (macro)monomers in parallel on the 100–500 mg scale, with each ROMP reaction taking ~5 min to reach completion (**Fig. 1a,b**, **Fig. S1-S11, Table S1-S4**). To demonstrate scalability of specific members of this library, several samples that displayed interesting mechanical properties were produced on the decagram scale with no purification steps required following polymerization. Comonomers **cHex**, **nHex**, and **nHexDec** differ by the identity of their aliphatic pendant groups, which vary in size, conformational freedom, and self-interaction. For statistical copolymers, graft densities of 0, 0.05, 0.1, 0.2, 0.3, 0.4, 0.5, 0.6, 0.7, 0.8, 0.9 and 1.0 were explored, the first and last of which represent homopolymers of the small-molecule and PDMS (macro)monomers, respectively. Diblock copolymer analogues were synthesized at grafting densities of 0.05, 0.2, 0.5 and 0.8. Two backbone degrees of polymerization (N_{bb}), 50 and 150, for each composition were prepared. For clarity, all copolymers are referred to by a sequence-**pendant**-N_{bb}-**grafting density** formalism. For example, a statistical copolymer with cyclohexyl pendant, N_{bb} of 50, and grafting density of 0.4 is referred to as stat-**cHex-50-0.4**.

This diversity-oriented approach allows for parallel tuning of grafting density, sequence, pendant composition, and N_{bb} (**Fig. 1b**), all of which play key roles in determining polymer conformations, self-interactions, and ultimately self-assembly and bulk properties. Specifically, grafting density influences backbone and side-chain flexibilities[42] and the volume fraction (f) of components. Statistical or block sequence influences domain spacing (d^*), chain conformations, and entanglement molecular weight.[12] N_{bb} determines number average molar mass (M_n) and backbone entanglements. Lastly, the comonomer pendant groups influence copolymer backbone flexibility and self-interaction. We note that side chain degree of polymerization (N_{sc}) was not varied in this study. Normalized size exclusion chromatography (SEC) traces for all statistical copolymers are shown in **Fig. 1c** and block samples in **Fig. S12-S17**. Copolymerization kinetics experiments[1,43] revealed that each of the three small-molecule comonomers copolymerize with Nb-PDMS with similar efficiency, yielding copolymers with slightly gradient monomer distributions that cannot explain differences in material properties (**Fig. S18-S26, Table S5**).

Room-Temperature Self-Assembly of Silicone-Based Graft Copolymers

To investigate the bulk morphologies of these graft (co)polymers, bulk samples were prepared by drop-casting from toluene solution and drying under vacuum at room temperature. The resulting materials were subjected to small angle X-ray scattering (SAXS, **Fig. 2a,b,e**, **Tables S1-S4**, and **Figs. S27-S48**) and, in some cases, transmission electron microscopy (TEM, **Figs. 2c,f** and **S49-S54**). In many cases, highly ordered morphologies, driven by phase separation of PDMS and the polynorbornene/comonomer backbone, were observed. Progressing from grafting density of 0.9 to 0.05 ($f_{PDMS-MM}$ from ~0.995 to ~0.53 for **cHex** and **nHex**, or 0.42 for **nHexDec** copolymers), and a concurrent transition from bottlebrush, to comb, to linear architecture (**Fig. 2a**), provided an array of morphologies including disordered (DIS), lamellar (LAM), hexagonally close packed cylinder (HEX), body centered cubic spherical (BCC), and long-range-disordered worm-like cylinders (D-CYL) as suggested by SAXS (**Fig. 2a**). While LAM, HEX, and D-CYL morphologies of bottlebrush and graft copolymers are well-documented, highly ordered BCC

morphologies are less common for densely grafted polymers.[39] Notably, BCC morphologies were not accessible to any of the diblock copolymers, nor were they observed in the **nHexDec** series, suggesting that backbone collapse, which is enabled by reductions in grafting density and/or with smaller comonomer pendants, is necessary to achieve this morphology.

Copolymers containing **cHex** and **nHex** displayed BCC or HEX morphologies at grafting densities of 0.7–0.1 while LAM morphologies were observed for all samples at grafting density of 0.05. Notably, the formation of LAM in the **nHexDec** series occurs at $f_{PDMS-MM}$ as high as 0.86, which is attributed to the steric bulk of the long aliphatic comonomer chains and the concomitant rigidification of the polynorbornene backbone. Lastly, the morphologies of the statistical copolymers are insensitive to N_{bb}, which agrees well with similar results observed for statistical and Janus bottlebrush multiblock copolymers (**Fig. 2a**).[3,4,38,44]

Interestingly, samples with highly ordered BCC morphology based on SAXS (**Fig. 2b**) appeared lamellar when analyzed by TEM (**Fig. 2c**). This observation could be due to a change in the material morphology due to thin-film confinement, or it could be the result of imaging a highly ordered BCC lattice from the (200) plane. To address this question, a select BCC sample, stat-**cHex-50-0.6** was studied with grazing-incidence small-angle X-ray scattering (GISAXS, **Fig. 2d**, **Figs. S55-S60**), which revealed significant surface anisotropy and confirmed the BCC morphology of the thin film (**Fig S61-S62)**. Samples with highly ordered LAM morphology based on SAXS (e.g., **Fig. 2e**) required microtoming prior to TEM imaging to visualize the lamellae (**Fig. 2f**). GISAXS of one such sample block-**nHexDec-150-0.05** showed well-ordered lamellae in plane to the surface of deposition (**Fig. 2g, S63-S64**).

To correlate the composition of each sample with morphological periodicity, domain spacing (d^*, nm, calculated as $10*(2\pi/q^*)$ where q^* is the principal scattering peak in $Å^{-1}$ measured by SAXS and 10 is a unit conversion factor) was plotted against grafting density for each sidechain sequence (statistical versus block), comonomer identity, and N_{bb} value (**Figs. 3a**,**b**). As expected,[3,5,44,45] while N_{bb} has little impact on d^* for the statistical copolymers, it has a large effect for the diblock copolymers (**Fig. 3a–c**) due to their tendency to assemble in side-to-side versus head-to-head orientations (**Fig. 3d**), respectively. The qualitatively different relationship between d^* and grafting density for diblock copolymers of N_{bb} = 50 versus 150 can be attributed to the presence of entanglements in the latter system when grafting density is below ~0.6 (*Note*: at this grafting density, the PNB homopolymer segment can become entangled; the entanglement molecular weight of linear polynorbornene with *n*-hexyl pendants was reported elsewhere as $N_{bb} \sim 45$).[46] Despite the considerable variations in morphology as a function of comonomer composition, the trends in d^* vs grafting density were similar for each comonomer, demonstrating that this simple copolymerization approach can provide facile access to materials with diverse morphologies and independently tunable d^* values from a simple set of (macro)monomer precursors.

Mechanical Properties of Graft Copolymer Silicones

Next, we sought to characterize the mechanical properties of select members of our graft copolymer library. First, we focused on samples that displayed the highly ordered BCC morphology, which behaved as transparent, soft, shear-thinning, viscoelastic solids despite their very high PDMS volume fractions ($f_{PDMS-MM}$ of ~0.98). Small-angle oscillatory shear rheology frequency (**Fig. 4a**) and temperature (**Fig. 4b**) sweeps of stat-**cHex-150-0.6** demonstrated a broad viscoelastic regime with a plateau storage modulus of 48 ± 9 kPa, which is similar to many soft biological tissues and softer than most commercial silicones. Notably, stat-**cHex-150-0.7**, which has an $f_{PDMS-MM}$ only 0.01 greater than for stat-**cHex-150-0.6**, was disordered (D-CYL) with a ~4 orders-of-magnitude lower G' (**Fig. S65**). To explain this large difference, we propose that the structure of our BCC samples most likely comprises the comonomer pendant groups and polynorbornene backbones closely packed in BCC cores embedded in an unbridged, rubbery PDMS matrix, forming plastic crystals where the lattice energy of the assembly provides physical crosslinking.[47–50] To this end, a rapid transition from viscoelastic solid to liquid is observed at 75 ± 1°C, which is consistent with the order-to-disorder transition (T_{ODT}) observed by variable-temperature SAXS (**Figs. 4c**). This transition underlies a shift from BCC to D-CYL, and though we note that the D-CYL arrangement does have short-range order, it is the loss of long-range order, as reflected by a morphology change and peak broadening, that causes us to denote this as an order-to-disorder transition, and not an order-to-order transition. The T_{ODT}s of the BCC samples prepared in this study ranged over ~20°C as a function of the graft copolymer composition, offering a strategy for tuning the processing conditions of these materials (**Fig. S66-S70**). Overall, these results highlight the advantages of our simple, diversity-oriented synthesis approach, enabling the discovery of emergent material properties from comparably small changes in polymer composition.

While the BCC samples described above formed ultrasoft materials, we noticed that LAM samples with low grafting densities (~0.05) formed unusually robust, albeit malleable, transparent solids (**Fig. 5a**), warranting further investigation. 5–10 g samples of *stat*-150-0.05 and *block*-150-0.05 copolymers with each pendant group were synthesized following similar procedures used for the library synthesis and were analyzed by dynamic mechanical analysis (DMA) and tensile testing.

DMA revealed that these samples behaved as thermoplastics with a wide range of properties including room temperature elastic moduli (E') up to ~150 MPa (**Fig. 5b**, **c**, **Fig. S71–S72**), which is similar to cartilage, tendons, and muscle tissues, is greater than commercial *crosslinked* silicones, and yet is softer than typical commodity thermoplastics. A remarkable dependence of E' on side chain sequence was observed, with the three statistical copolymers displaying much higher values than their block copolymer counterparts. For example, stat-**150-0.05-cHex** has a ~15-fold greater E' than block-**150-0.05-cHex** despite their identical composition (**Fig. 5b**). Given that these samples are not chemically crosslinked and are expected to have few entanglements (at most 1 entanglement per polynorbornene block in the case of blocky samples), their disparate mechanical properties can be explained by the much greater density of high-energy phase boundaries in the statistical copolymer, as reflected by their lower d^*.

Notably, the thermal transitions of these materials were not sequence dependent, changing by only ~10% between statistical and block samples, and were not related to T_{ODT}s (**Fig. S73-S89, Table S6**). Instead, they were dominated by the glass transition temperatures of the small molecule norbornene homopolymers ($T_{g,PNB}$) with **cHex** > **nHex** > **nHexDec** (201 ± 4, 95 ± 1, 64 ± 1°C respectively). The comonomers also had a major effect on *E'*, decreasing from ~150 MPa to ~100 MPa to ~50 MPa from **cHex** to **nHexDec** to **nHex**, respectively. These findings demonstrate using comonomer composition to broadly tune the properties of these silicone thermoplastics.

Universal tensile testing was conducted on the three statistical graft copolymer samples with different comonomer pendants (**Fig. 5d–i**) (*Note*: due to their lack of entanglement and limited PDMS interdigitation, **Fig. 3d**, the block copolymer samples were too brittle to acquire meaningful data). The Young's moduli (*E*, **Fig. 5f**) trended with the storage moduli obtained by DMA. Interestingly, the comonomer pendant composition had major impacts on the ultimate tensile strength (**Fig. 5g**), strain at break (**Fig. 5h**), and toughness (**Fig. 5i**, approximated by the area underneath the stress–strain curves). For example, strain at break ranged from a remarkable 230 ± 54% to 57 ± 5% to only 16 ± 1% for **nHexDec**, **cHex**, and **nHex** samples, respectively. Tensile strength ranged from 2.4 ± 0.2 (**nHexDec**) to 6.3 ± 0.2 (**cHex**) MPa, on par with commercial silicone elastomers such as Sylgard 184 (ultimate tensile strength c.a. 6.8 MPa).[40] Similarly, toughness varied from ~600 J•m^{-3} to ~300 J•m^{-3} to ~50 J•m^{-3} across these samples. Altogether, these differences are attributed to a combination of the pendant group self-interaction strength, space-filling, and ability to undergo structural rearrangements during extension. Additionally, given that these samples are uncrosslinked, we expected that they could be recycled similarly to other thermoplastics. To demonstrate this concept, an **nHexDec**-based sample was dissolved, recast into a dogbone shape, and subjected to tensile testing. This process could be repeated at least 3 times with negligible impact on tensile properties (**Fig. S90**).

Summary and Outlook

Herein, we investigated the impact of comonomer composition on graft (co)polymer-based silicones using a novel diversity-oriented synthesis approach. Using one PDMS macromonomer and three comonomers that differed only by their aliphatic pendants, a library of 92 (co)polymers with varied sequence, backbone length, grafting density, and comonomer composition was synthesized. Characterization of this library confirmed many well-established trends in graft copolymer assembly, but also revealed unprecedented and dramatic variations in material properties that correlated with comonomer composition and sequence, offering a new and simple strategy to target bespoke material properties. Moreover, members of this library displayed properties that span the entire gamut of silicones properties, with certain features surpassing those of commercial systems; for example, a new class of transparent, reprocessable silicone thermoplastics with stiffness and toughness that surpass unfilled, crosslinked silicones as well as classical rubbers (e.g., ABS/SBS formulations) was discovered. Looking forward, we note that while the impacts of comonomers in this system are undeniable, the precise molecular mechanisms that translate from pendant composition to microphase morphology to bulk

properties remains to be elucidated. In the future, this general approach should be applicable to a range of chemical systems in addition to silicones.

Declarations

Data Availability

All data supporting the findings of this study are available within the article and the Supplementary Information, and/or from the corresponding author upon reasonable request.

Author Contributions

K. E. L. H. and J. A. J. conceived of the idea. K. E. L. H., D. K. and A. H.-A. synthesized materials and characterized copolymers. K. E. L. H., A. H.-A., and W. Z. conducted materials characterization. A. J. F. conducted cryo-microtome TEM imaging. A. L. conducted GISAXS measurements. K. E. L. H. and J. A. J. wrote the manuscript. All authors read and revised the manuscript.

Acknowledgements

This work was supported by DOW. The authors would specifically like to thank Dr. Rocky Zhu, and Dr. Zachary Kean for their contributions. The authors would like to thank Dr. Byeongdu Lee (Argonne National Lab) for assistance with SAXS measurements, Yazhen Xue (Yale) for indexing of GISAXS data, and Zehao Sun (MIT) for helpful discussion.

Competing interests

The authors declare no competing interests.

Author information

Correspondence and requests for materials should be sent to J.A.J. (jaj2109@mit.edu)

References

1. B. Chang, A. *et al.* Design, Synthesis, and Self-Assembly of Polymers with Tailored Graft Distributions. *J. Am. Chem. Soc.* **139**, 17683–17693 (2017).
2. Jiang, L., Nykypanchuk, D., J. Pastore, V. & Rzayev, J. Morphological Behavior of Compositionally Gradient Polystyrene–Polylactide Bottlebrush Copolymers. *Macromolecules* **0**, (2019).
3. Cheng, L.-C. *et al.* Templated Self-Assembly of a PS-Branch-PDMS Bottlebrush Copolymer. *Nano Lett.* **18**, 4360–4369 (2018).
4. Kawamoto, K. *et al.* Graft-through Synthesis and Assembly of Janus Bottlebrush Polymers from A-Branch-B Diblock Macromonomers. *J. Am. Chem. Soc.* **138**, 11501–11504 (2016).

5. Xia, Y., D. Olsen, B., A. Kornfield, J. & H. Grubbs, R. Efficient Synthesis of Narrowly Dispersed Brush Copolymers and Study of Their Assemblies: The Importance of Side Chain Arrangement. *J. Am. Chem. Soc.* **131**, 18525–18532 (2009).
6. Gai, Y., Song, D.-P., M. Yavitt, B. & J. Watkins, J. Polystyrene-block-poly(ethylene oxide) Bottlebrush Block Copolymer Morphology Transitions: Influence of Side Chain Length and Volume Fraction. *Macromolecules* **50**, 1503–1511 (2017).
7. Lin, T.-P. *et al.* Effects of Grafting Density on Block Polymer Self-Assembly: From Linear to Bottlebrush. *ACS Nano* **11**, 11632–11641 (2017).
8. Haugan, I. N. *et al.* Consequences of Grafting Density on the Linear Viscoelastic Behavior of Graft Polymers. *ACS Macro Lett.* **7**, 525–530 (2018).
9. Fei, H.-F. *et al.* Influence of Molecular Architecture and Chain Flexibility on the Phase Map of Polystyrene-block-poly(dimethylsiloxane) Brush Block Copolymers. *Macromolecules* **52**, 6449–6457 (2019).
10. Abbasi, M., Faust, L. & Wilhelm, M. Comb and Bottlebrush Polymers with Superior Rheological and Mechanical Properties. *Adv. Mater.* **31**, (2019).
11. Roovers, J. & W. Graessley, W. Melt rheology of some model comb polystyrenes. *Macromolecules* **14**, 766–773 (2002).
12. R. López-Barrón, C., H. Tsou, A., R. Hagadorn, J. & A. Throckmorton, J. Highly Entangled α-Olefin Molecular Bottlebrushes: Melt Structure, Linear Rheology, and Interchain Friction Mechanism. *Macromolecules* **51**, 6958–6966 (2018).
13. Liang, H. *et al.* Universality of the Entanglement Plateau Modulus of Comb and Bottlebrush Polymer Melts. *Macromolecules* **51**, 10028–10039 (2018).
14. Liang, H., Cao, Z., Wang, Z., S. Sheiko, S. & V. Dobrynin, A. Combs and Bottlebrushes in a Melt. *Macromolecules* **50**, 3430–3437 (2017).
15. Verduzco, R., Li, X., Pesek, S. L. & Stein, G. E. Structure, function, self-assembly, and applications of bottlebrush copolymers. *Chem. Soc. Rev.* **44**, 2405–2420 (2015).
16. J. Dalsin, S. *et al.* Bottlebrush Block Polymers: Quantitative Theory and Experiments. *ACS Nano* **9**, 12233–12245 (2015).
17. Brett Runge, M. & B. Bowden, N. Synthesis of High Molecular Weight Comb Block Copolymers and Their Assembly into Ordered Morphologies in the Solid State. *J. Am. Chem. Soc.* **129**, 10551–10560 (2007).
18. Rzayev, J. Molecular Bottlebrushes: New Opportunities in Nanomaterials Fabrication. *ACS Macro Lett.* **1**, 1146–1149 (2012).
19. B. Zhulina, E., S. Sheiko, S., V. Dobrynin, A. & V. Borisov, O. Microphase Segregation in the Melts of Bottlebrush Block Copolymers. *Macromolecules* **0**, (2020).
20. Chremos, A. & E. Theodorakis, P. Morphologies of Bottle-Brush Block Copolymers. *ACS Macro Lett.* **3**, 1096–1100 (2014).

21. Xie, G., R. Martinez, M., Olszewski, M., S. Sheiko, S. & Matyjaszewski, K. Molecular Bottlebrushes as Novel Materials. *Biomacromolecules* **20**, 27–54 (2018).
22. Liberman-Martin, A. L., Chu, C. K. & Grubbs, R. H. Application of Bottlebrush Block Copolymers as Photonic Crystals. *Macromol. Rapid Commun.* **38**, 1–15 (2017).
23. Song, D.-P., H. Zhao, T., Guidetti, G., Vignolini, S. & M. Parker, R. Hierarchical Photonic Pigments via the Confined Self-Assembly of Bottlebrush Block Copolymers. *ACS Nano* **13**, 1764–1771 (2019).
24. Daniel, W. F. M. *et al.* Solvent-free, supersoft and superelastic bottlebrush melts and networks. *Nat. Mater.* **15**, 183–189 (2016).
25. Mukumoto, K. *et al.* Phototunable Supersoft Elastomers using Coumarin Functionalized Molecular Bottlebrushes for Cell-Surface Interactions Study. *Macromolecules* **47**, 7852–7857 (2014).
26. Liang, H., S. Sheiko, S. & V. Dobrynin, A. Supersoft and Hyperelastic Polymer Networks with Brushlike Strands. *Macromolecules* **51**, 638–645 (2018).
27. Liang, H., Wang, Z. & V. Dobrynin, A. Strain-Adaptive Self-Assembled Networks of Linear-Bottlebrush-Linear Copolymers. *Macromolecules* **0**, (2019).
28. Nian, S. *et al.* Molecular Architecture Directs Linear–Bottlebrush–Linear Triblock Copolymers to Self-Assemble to Soft Reprocessable Elastomers. *ACS Macro Lett.* **0**, 1528–1534 (2019).
29. Vohidov, F. *et al.* Design of BET Inhibitor Bottlebrush Prodrugs with Superior Efficacy and Devoid of Systemic Toxicities. *J. Am. Chem. Soc.* **143**, 4714–4724 (2021).
30. Liao, L. *et al.* A Convergent Synthetic Platform for Single-Nanoparticle Combination Cancer Therapy: Ratiometric Loading and Controlled Release of Cisplatin, Doxorubicin, and Camptothecin. *J. Am. Chem. Soc.* **136**, 5896–5899 (2014).
31. Vatankhah-Varnosfaderani, M. *et al.* Mimicking biological stress–strain behaviour with synthetic elastomers. *Nature* **549**, 497–501 (2017).
32. Sarkar, S., Lightfoot-Vidal, S. E., Schauer, C. L., Vresilovic, E. & Marcolongo, M. Terminal-end functionalization of chondroitin sulfate for the synthesis of biomimetic proteoglycans. *Carbohydr. Polym.* **90**, 431–440 (2012).
33. N. Keith, A. *et al.* Bottlebrush Bridge between Soft Gels and Firm Tissues. *ACS Cent. Sci.* **0**, (2020).
34. Vatankhah-Varnosfaderani, M. *et al.* Chameleon-like elastomers with molecularly encoded strain-adaptive stiffening and coloration. *Science (80-.).* **359**, 1509–1513 (2018).
35. Gopal Goswami, K. *et al.* Self-Assembly of Amphiphilic Copolymers with Sequence-Controlled Alternating Hydrophilic–Hydrophobic Pendant Side Chains. *ACS Appl. Polym. Mater.* **2**, 2035–2045 (2020).
36. Hattori, G., Hirai, Y., Sawamoto, M. & Terashima, T. Self-assembly of PEG/dodecyl-graft amphiphilic copolymers in water: Consequences of the monomer sequence and chain flexibility on uniform micelles. *Polym. Chem.* **8**, 7248–7259 (2017).
37. Jiang, Z., Liu, H., He, H., E. Ribbe, A. & Thayumanavan, S. Blended Assemblies of Amphiphilic Random and Block Copolymers for Tunable Encapsulation and Release of Hydrophobic Guest

Molecules. *Macromolecules* **0**, (2020).

38. Matsumoto, M., Terashima, T., Matsumoto, K., Takenaka, M. & Sawamoto, M. Compartmentalization Technologies via Self-Assembly and Cross-Linking of Amphiphilic Random Block Copolymers in Water. *J. Am. Chem. Soc.* **139**, 7164–7167 (2017).
39. Xie, R. *et al.* Room temperature 3D printing of super-soft and solvent-free elastomers. 1–11 (2020).
40. Johnston, I. D., McCluskey, D. K., Tan, C. K. L. & Tracey, M. C. Mechanical characterization of bulk Sylgard 184 for microfluidics and microengineering. *J. Micromechanics Microengineering* **24**, (2014).
41. Bielawski, C. W. & Grubbs, R. H. Living ring-opening metathesis polymerization. *Progress in Polymer Science (Oxford)* (2007). doi:10.1016/j.progpolymsci.2006.08.006
42. M. Yavitt, B. *et al.* Long-Range Lamellar Alignment in Diblock Bottlebrush Copolymers via Controlled Oscillatory Shear. *Macromolecules* **53**, 2834–2840 (2020).
43. Lin, T.-P. *et al.* Control of Grafting Density and Distribution in Graft Polymers by Living Ring-Opening Metathesis Copolymerization. *J. Am. Chem. Soc.* **139**, 3896–3903 (2017).
44. V.-T. Nguyen, H. *et al.* Scalable Synthesis of Multivalent Macromonomers for ROMP. *ACS Macro Lett.* **7**, 472–476 (2018).
45. M. Bates, C., B. Chang, A., Momčilović, N., C. Jones, S. & H. Grubbs, R. ABA Triblock Brush Polymers: Synthesis, Self-Assembly, Conductivity, and Rheological Properties. *Macromolecules* **48**, 4967–4973 (2015).
46. M. Boyle, B., Heinz, O., M. Miyake, G. & Ding, Y. Impact of the Pendant Group on the Chain Conformation and Bulk Properties of Norbornene Imide-Based Polymers. *Macromolecules* **52**, 3426–3434 (2019).
47. P. Marencic, A., W. Wu, M., A. Register, R. & M. Chaikin, P. Orientational Order in Sphere-Forming Block Copolymer Thin Films Aligned under Shear. *Macromolecules* **40**, 7299–7305 (2007).
48. M. Sebastian, J., Lai, C., W. Graessley, W. & A. Register, R. Steady-Shear Rheology of Block Copolymer Melts and Concentrated Solutions: Disordering Stress in Body-Centered-Cubic Systems. *Macromolecules* **35**, 2707–2713 (2002).
49. Timmermans, J. Plastic crystals: a historical overview. *J. Phys. Chem. Solids* **18**, 1–8 (1961).
50. Macfarlane, D. R., Huang, J. & Forsyth, M. Lithium-doped plastic crystal electrolytes exhibiting fast ion conduction for secondary batteries. *Nature* **402**, 792–794 (1999).

Figures

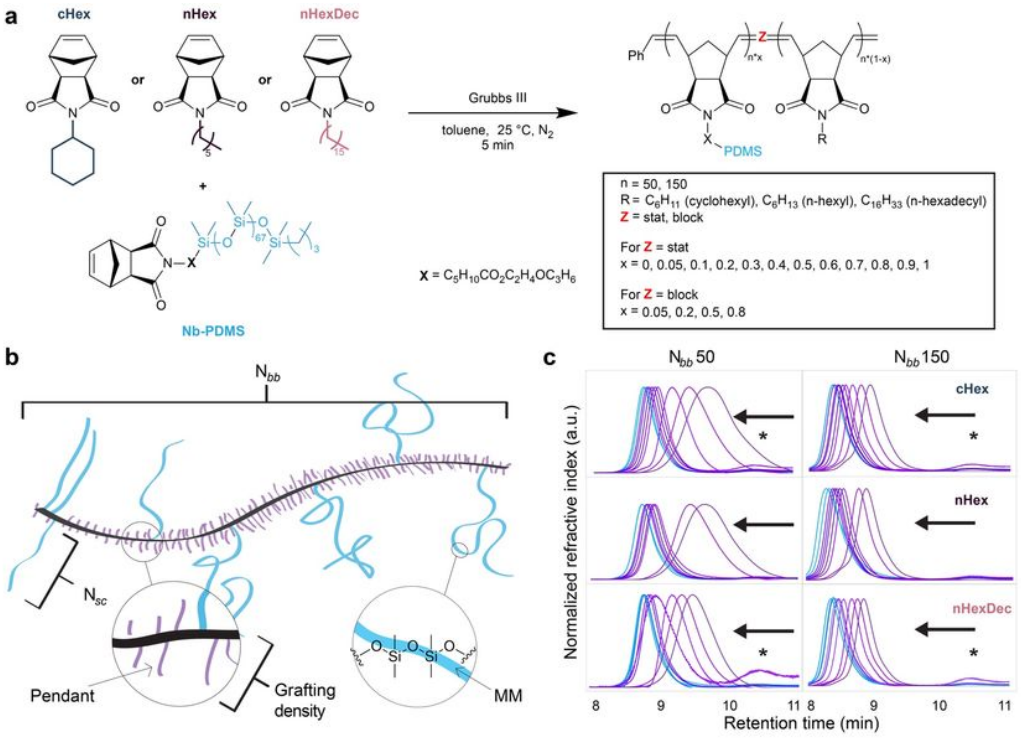

Figure 1

Synthesis of a library of graft copolymers. a, Graft copolymers comprising polynorbornene backbones, PDMS arms (Nb-PDMS), and small-molecule comonomer pendants (**cHex**, **nHex**, or **nHexDec**) are prepared by one-step Ru-initiated ROMP. **b**, Schematic representation of the graft copolymer architecture, emphasizing the role of pendant groups. **c**, Size exclusion chromatography refractive index traces of *statistical* graft copolymers. Arrows indicate direction of increasing grafting density. ***nHex**-containing polymers at grafting density = 0.2 are isorefractive with chloroform and could not be detected. **cHex** and **nHexDec** copolymers at grafting density = 0.2 are nearly isorefractive with chloroform, resulting in an exaggerated residual macromonomer signal despite >99.9% conversion by NMR (retention time ~10.5 minutes).

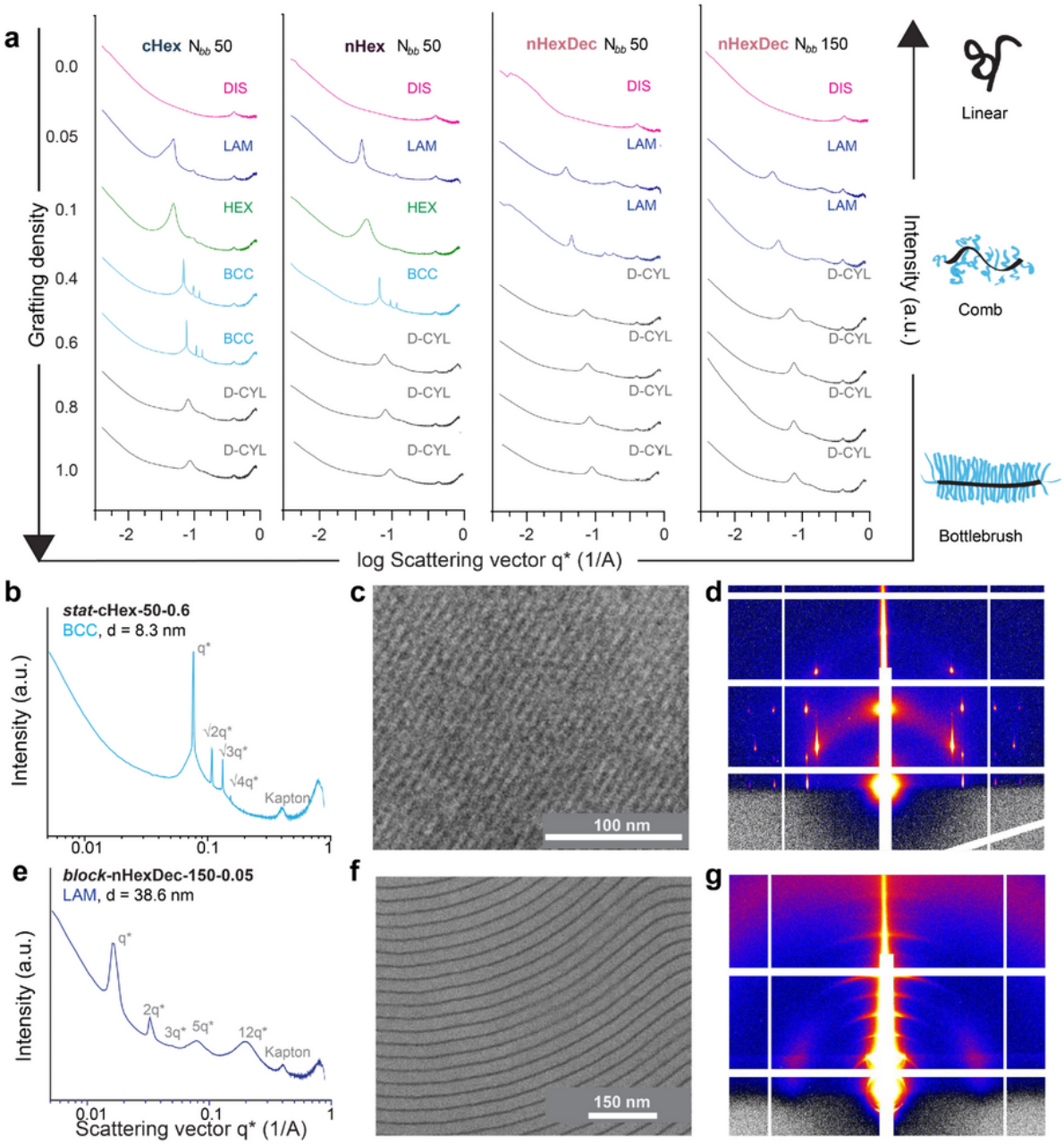

Figure 2

Self-assembly and surface effects of pendant-modified statistical graft copolymers. a, 1D SAXS curves of statistical copolymers. DIS = disordered, LAM = lamellar, HEX = hexagonally packed cylinders, BCC = body-centered cubic, D-CYL = long-range-disordered worm-like cylinders. **b**, 1D SAXS of ***stat*-cHex-50-0.6**. **c**, TEM image of ***stat*-cHex-50-0.6** shows apparent lamellae. **d**, GISAXS of ***stat*-cHex-50-0.6** shows highly ordered anisotropic surface assembly; **e**, 1D SAXS of ***block*-nHexDec-150-0.05**. **f,** Cryo-microtome TEM

image of ***block*-nHexDec-150-0.05**. **g**, GISAXS of ***block*-nHexDec-150-0.05** shows highly ordered lamellae in thin film parallel to surface.

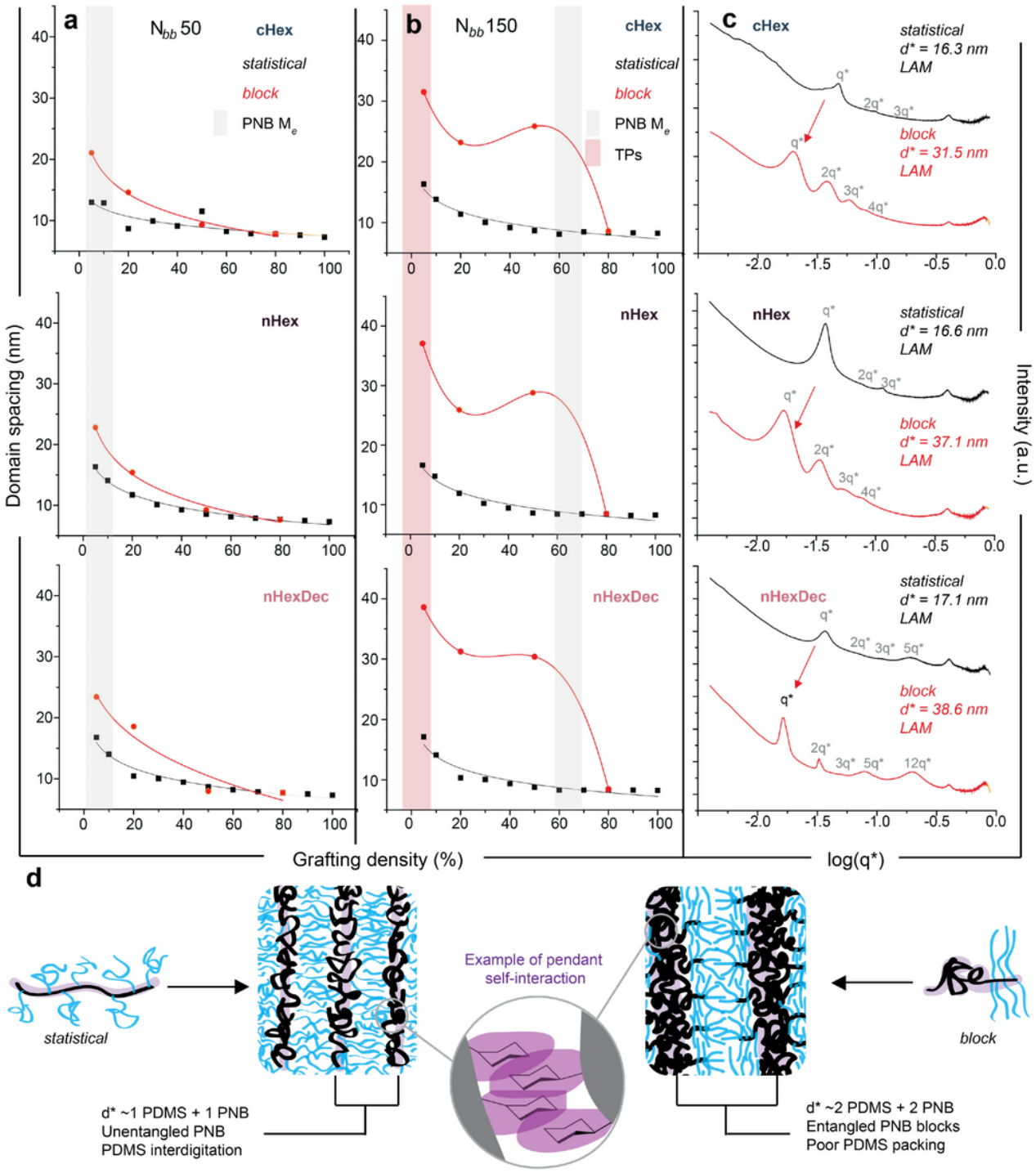

Figure 3

Influence of molecular architecture on domain spacing. a,b. Domain spacing vs grafting density for N_{bb} = 50 copolymers, separated by small molecule comonomer and overlaid by architecture. Black lines are given by a power law function, red lines by an arbitrary cubic. Gray rectangles denote approximate entanglement degree of polymerization of linear polynorbornene homopolymer. Red rectangle highlights 6 TP samples analyzed further. **c**, 1D SAXS curves of six TP-forming samples (highlighted by the red rectangle in **b**), (N_{bb} = 150, grafting density = 0.05) showing approximate doubling of domain spacing of *block* vs *stat* samples. **d**, Illustration of molecular process underlying doubling of domain spacing in blocky samples above entanglement threshold.

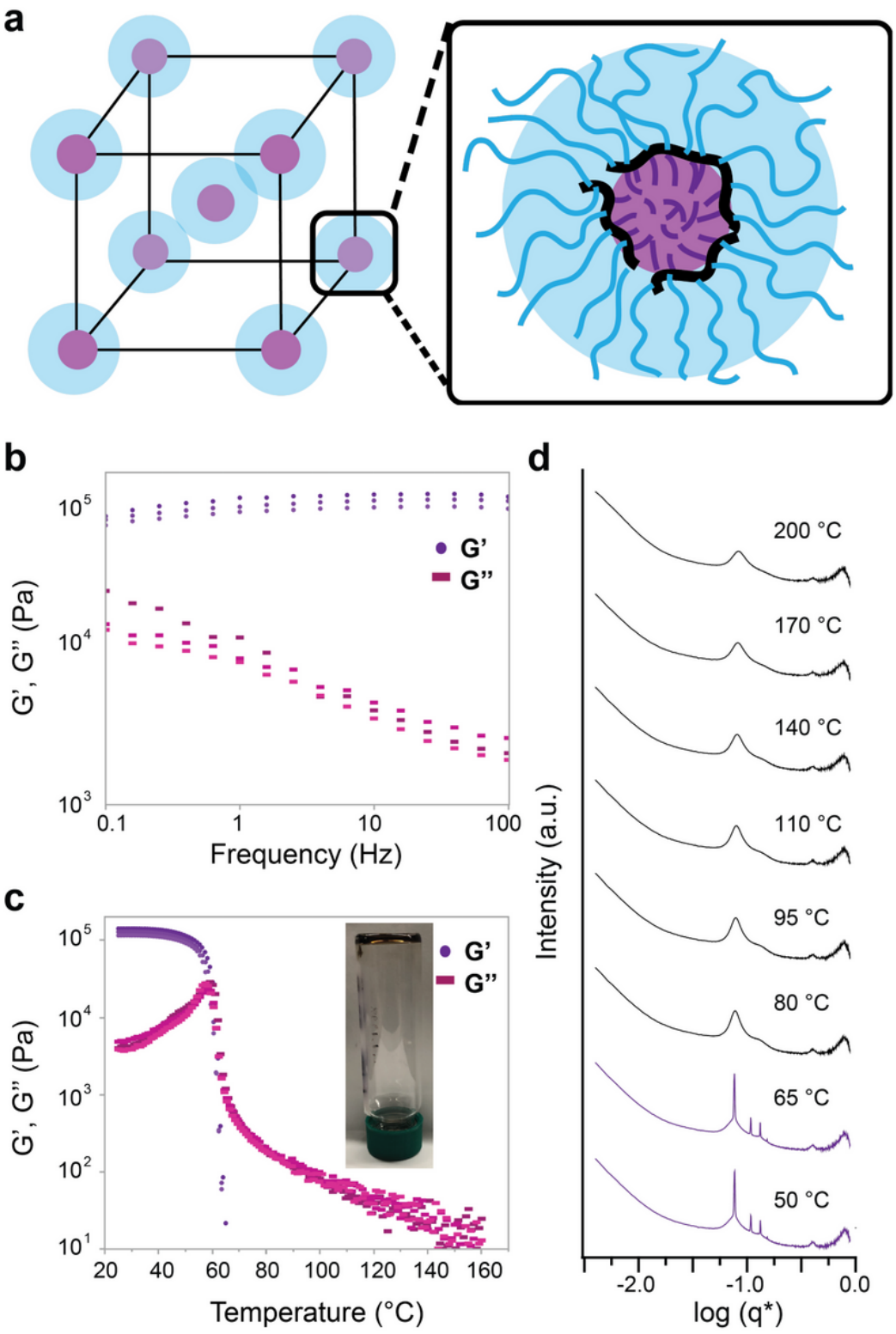

Figure 4

Rheological characterization of representative BCC sample, *stat*-cHex-50-0.4. a. Schematic depicting polymer conformation in BCC morphology. **b**, Frequency sweep rheology shows a broad linear viscoelastic regime. **c.** Temperature sweep rheology highlights sharp transition from viscoelastic solid to liquid. Inset: inverted vial showing viscoelastic solid behavior of sample. **d**. Variable-temperature SAXS

reveals an order-disorder transition temperature between 65 and 80 °C, in agreement with the transition noted in **b**.

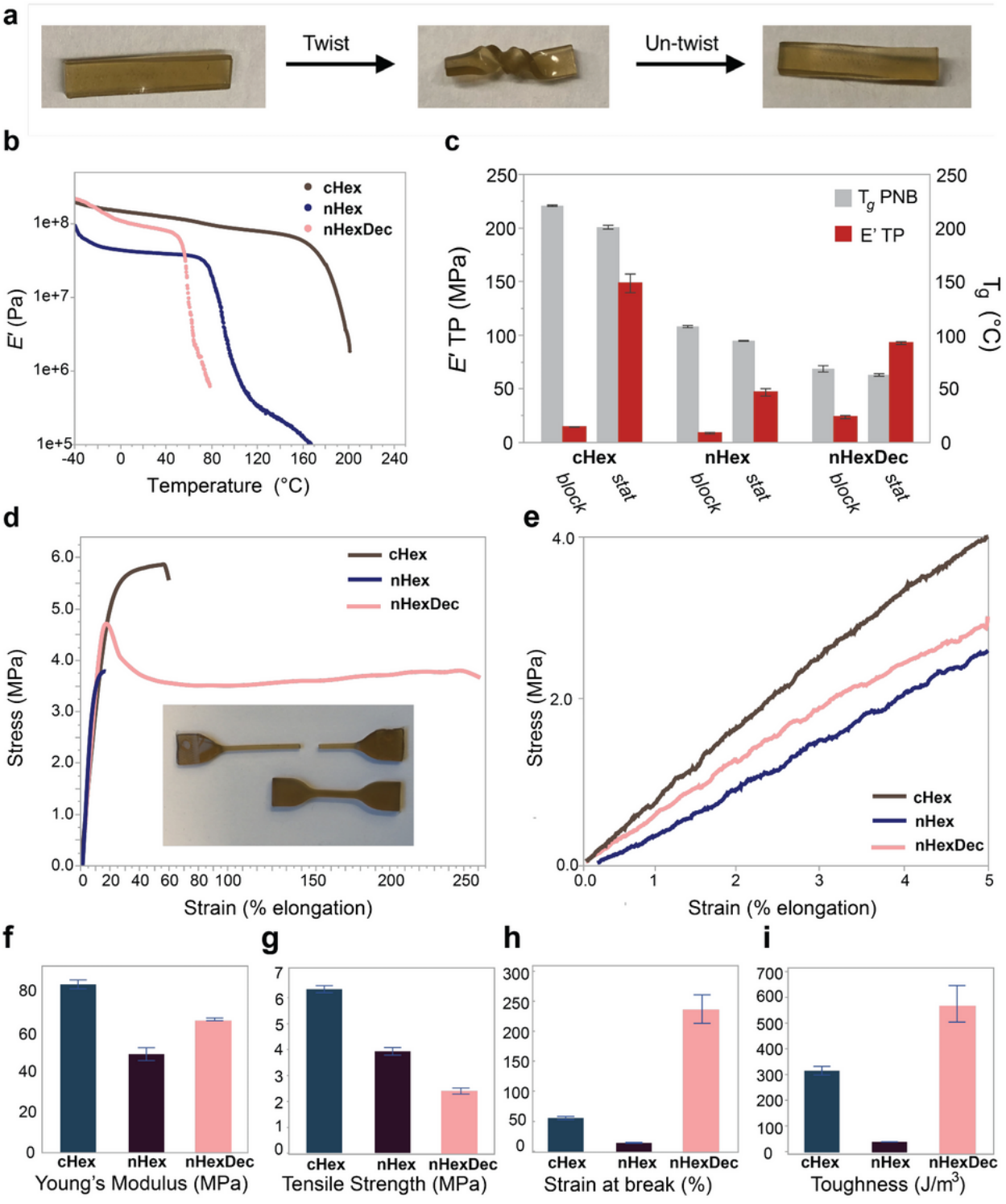

g

Figure 5

Thermomechanical performance of lamellar TPs. a, Samples can be deformed and hold their shape after deformation (sample shown is **stat-nHexDec-150-0.05**). **b**, Stacked *E'* plots from DMA temperature sweeps of *stat*-150-0.05 samples demonstrate pendant-sensitive modulus and glass transition temperature. **c**, Tabulated *E'* (at 298 K) and $T_{g,PNB}$ (from maximum in tan(delta)) as measured by DMA. **d**, Overlaid representative stress-strain curves of *stat* lamellar TPs. Inset: **nHexDec** tensile samples before (bottom) and after (top) tensile testing to failure. **e**, Close-up of first 3% of strain during tensile testing used to obtain relative Young's moduli. **f-i**, Mechanical properties as obtained from stress-strain curves in triplicate), **f**, Young's modulus (MPa) **g**, Ultimate tensile strength (MPa) **h**, Strain at break (%), **i**, Toughness (J m^{-3}). Error bars represent standard error.

Supplementary Files

This is a list of supplementary files associated with this preprint. Click to download.

- 02SelfAssemblySIkh14slk02jj04mz01dow01wz01aha02.pdf